Al-Khwarizmi Engineering Journal, Vol. 9, No. 3, P.P. 38- 57 (2013)

Al-Khwarizmi Engineering Journal

Theoretical and Practical Investigation of Blood Flow through Stenosed Coronary Lad Artery

Sadiq J. Abbass[*] **Furman K. Ahmed**[**] **Zahraa A. Mohammed**[***]

[*]*Department of Medical Engineering / College of Engineering / Al-Nahrain University*

[**]*Department of Engineering / Nursing Home Hospital*

[***]*Department of Biomedical Engineering /Al-Khwarizmi College of Engineering / University of Baghdad*

(Received 14 February 2012; accepted 11 September 2013)

Abstract

Atherosclerosis is the most common causes of vascular diseases and it is associated with a restriction in the lumen of blood vessels. So; the study of blood flow in arteries is very important to understand the relation between hemodynamic characteristics of blood flow and the occurrence of atherosclerosis.

looking for the physical factors and correlations that explain the phenomena of existence the atherosclerosis disease in the proximal site of LAD artery in some people rather than others is achieved in this study by analysis data from coronary angiography as well as estimating the blood velocity from coronary angiography scans without having a required data on velocity by using some mathematical equations and physical laws. Fifty-eight patients were included in this study that underwent cardiac catheterization for diagnostic coronary angiography. It found some information that may explain the ability of small arteries to develop the lesions with time mainly in proximal site of LAD artery.

For investigation the fluid-structural response to pulsatile Newtonian and non-Newtonian blood flow through an axisymmetric stenosed coronary artery; the theoretical simulation is built up by using ANSYS 11, to evaluate the biomechanical parameters in the atherosclerotic process. Rigid and Newtonian cases were investigated to provide an understanding on the effects of incorporating the Fluid-Structural Interaction (FSI) into the model. For validation of the models and methods used, the computation results are compared with the previous studies. The non-Newtonian Carreau model was investigated with FSI, which showed a little difference in comparison with the Newtonian flow model in terms of velocity, pressure, wall shear stress (WSS), and stress distribution.

Keywords: *blood flow, atherosclerosis, stenosed artery, simulation, modeling, coronary angiography.*

1. Introduction

Understanding of blood flow hemodynamics has great importance in testing the hypothesis of disease pathogenesis, assessment and diagnosis of the cardiovascular disease, vascular surgery planning, modeling the transport of drugs through the circulatory systems and determining their local concentrations, predicting the performance of cardiovascular equipments or instruments that have not yet been built such as heart valves, stents, probes, etc., and devising better therapies of mainly coronary artery occluding, atherosclerosis, thromboses, vacuities or varicose, aneurysms, etc. [1]

Recently there has been a significant amount of researches done on stenosed arteries; arteries that have blockage caused by a disease called atherosclerosis. The term arterial stenosis refers to the narrowing of an artery where the internal cross sectional area (lumen) of blood vessel reduces.

In the atherosclerotic disease the certain cholesterols and other lipids are deposited beneath the intima (inner lining) of the arterial wall which is normally smooth to allow for easy transportation of red blood cells, oxygen white blood cell, nutrients, and other vital substances that the body required. As the amount of this fatty material increases there is an accompanying proliferation of connective tissue and the whole

forms a thickened area in the vessel wall called plaque. [2]

Atherosclerosis can affect all large and medium-sized arteries, including the coronary, carotid, and cerebral arteries. Risk factors for this disease include diabetes, cigarette smoking, family history, sedentary lifestyle and hypertension. [3]

Most of the studies available at present focus on the clinical aspects of the disease. There has been a great push, however, to understand the physics involved with the disease itself, including the cause and possible methods of treating it. The focusing on some of these physical factors for putting our hand on some individual properties that, directly or indirectly, may be have an influence on existing the atherosclerotic disease in some people rather the others and in some arteries rather the others, is the aims that this study wants to do.

Also, the computational techniques have demonstrated a strong ability in modeling flow behavior within stenosed arteries of varying geometries and conditions that can be specified according to realistic conditions.[4]

In this study, the incorporation of two factors, i.e. non-Newtonian blood flow and FSI (fluid-structural interaction) , is achieved to investigate the pulsatile flow behavior in stenosed artery as well as the structural response.

2. Aims of Study

The stenosis in coronary arteries due to atherosclerotic disease may prevent the blood flow and causes a heart attack or death in its acute situation.[4]

Therefore it is very important to know how blood is flowing in the area of stenosis, then that will help doctors or surgeons to make a diagnosis or to make an operation plan. The proximal segment of LAD artery is selected in this study for being a region of interest where atherosclerosis is likely to occur.

The First Aim of the work described in this paper is the investigation of the fluid structural response to pulsatile Newtonian and non-Newtonian blood flow through an axisymmetric stenosed vessel which has similar LAD coronary artery dimensions by using the CFD (computational fluid dynamics) technique, for providing a basic understanding of atherosclerosis. Among various constitutive equations, the non-Newtonian Carreau model is used to determine its non-Newtonian influence as well as the basic physical characteristics such as stresses.

The Second Approach to investigate the blood flow in stenosed LAD coronary artery is by performing the coronary angiography on real cases that were found at two hospitals in Baghdad. However, in this way a qualitative assessment is made for understanding the physiological significance of disease and trying to estimate the blood velocity from coronary angiography scans without having the required data on velocity by using some mathematical equations and physical laws, as well as, looking for any other physical factors and correlations which explain the lesion in the proximal site of (LAD).

3. Angiographical Investigation

3.1. The Patients

Fifty-eight patients were included in this study and divided into two groups; Group I: consisted of fifteen individuals; (4) females and (11) males who underwent cardiac catheterization for a typical chest pain and the diameter stenosis in proximal LAD was less than 25%, so they were considered a control group. Group II: consisted of forty-three patients; (10) females and (33) males with the diameter stenosis of more than 25% in proximal LAD.

In the catheterization laboratory, the measurements were done by performing coronary angiography on the real cases found at two hospitals in Baghdad, and by injecting a contrast medium; the cardiac coronary arteries were made visible on X-ray film.

The main clinical characteristics of the patients enrolled in this study are summarized in Table (1) and the comparison in risk factors between two groups is shown in the Figure (1).

Table 1,
Patients' clinical characteristics.

Characteristics	Group I (n = 15)	Group II (n = 43)
Age, range	(46 – 58)	(54 –81)
Male sex, n (%)	11 (73)	33 (77)
Body weight (kg)	61.4 + 5.3	64 + 6.6
Risk factors, n (%)		
Family history	4 (27)	31 (72)
Diabetes	2 (13)	10 (23)
Smoking habits	4 (27)	29 (67)

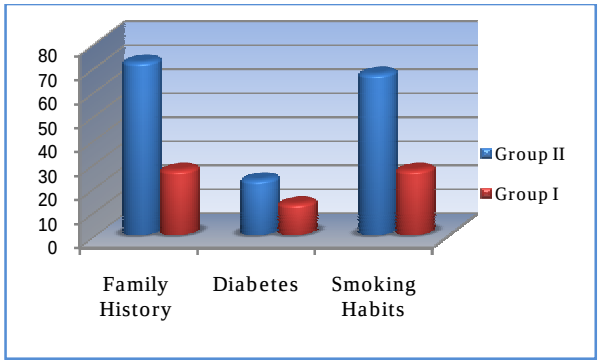

Fig. 1. The Comparison in Risk Factors between Two Groups.

3.2. Statistical Analyses and the Obtained Data

Statistical analysis in this study was done using SPSS 11.5 software. The statistical significance of difference in mean of a continuous dependent (normally distributed variable) between two groups was assessed by independent samples t-test. P values of $\leq$ 0.05 were statistically significant. In biological system the average is the value taken for the most numbers in the study and the standard deviation (±SD) reflects the range around the average.

The reference diameters, cross section areas, and normal blood flow rate at the proximal site of (LAD) for all patients were obtained from the angiograms are illustrated in Table (2) and (3).

Table 2,
Values of diameters, cross section areas and flow rates of the proximal site of LAD in groups (I & II).

	Group I Mean ± SD (min – max)	Group II Mean ± SD(min – max)	P Value
Diameter (mm)	3.48 ± 0.30 (2.86 - 3.81)	3.26 ± 0.25 (2.63 - 3.78)	0.04*
Cross Section Area (mm^2)	10.00 ± 1.55 (6.43 – 11.5)	8.50 ± 1.38 (5.50 – 11.20)	0.04*
Flow Rate (ml/s)	1.91 ± 0.31 (1.29 - 2.22)	1.72 ± 0.18 (1.10 – 1.98)	0.05*

Table 3,
The values of diameters, cross section areas, and flow rates of the proximal site of LAD in (males & females) of groups (I & II).

	Males		P value	Females		P value
	Group I Mean ± SD	Group II Mean ± SD		Group I Mean ± SD	Group II Mean ± SD	
Diameter (mm)	3.53 ± 0.30	3.28 ± 0.26	0.033*	3.34 ± 0.21	3.29 ± 0.30	0.80
Cross Section Area (mm^2)	9.87 ± 1.63	8.51 ± 1.40	0.030*	8.78 ± 1.17	8.53 ± 1.46	0.80
Flow Rate (ml/s)	1.97 ± 0.33	1.70 ± 0.28	0.034*	1.76 ± 0.24	1.72 ± 0.29	0.82

3.3. Calculations and Data Collection

There were many physical parameters involved in the study, they were based on the manual of the medical system existed in hospital. The measurements were done as follows:

The reference (diameter in mm and cross section area in mm^2) and obstructed (diameter in mm and cross section area in mm^2) for the proximal segment of LAD were calculated for each patient by the provided software. The cross section area calculation is based on the assumption of circular cross section at the obstruction and reference position.

For abnormal patients, the lesion length (mm) was calculated by the provided software.

The normal flow (ml/s) is calculated for each patient from the reference cross section area (cm^2) of the vessel and an assumed average flow velocity of (20 cm/s) by using the equation below:

$$Q = U\,A \quad \ldots(1)$$

- Symmetry index was given by the provided software. It grades a plaque area in term of its position around the internal wall of the artery on a 1.0 that means the plaque area is completely symmetric and 0.0 means the plaque area is totally eccentric.

Percentage diameters and area stenosis can be calculated by using the following equations:

$$\%\ D\ stenosis = \left(1 - \frac{D_{Obstruction}}{D_{Reference}}\right) \times 100\ \% \quad \ldots(2)$$

$$\%\ A\ stenosis = \left(1 - \frac{A_{Obstruction}}{A_{Reference}}\right) \times 100\ \% \quad \ldots(3)$$

The value of ΔP was determined by the provided software, based on the fluid dynamic equations and validated in-vitro by Young and in-vivo by Gould:

$$\Delta P = Cv.\,Flow + Ct.\,(Flow)^2 \quad \ldots(4)$$

Where:

ΔP = Pressure drop. Cv=Poiseuille resistance in function of stenotic length. Ct = Turbulence resistance in function of stenosis (experimental value).

Flow = (20 cm/s × reference area (cm^2)) × SFR ratio

- The SFR ratio means stenotic flow reserve. Stenoses cause problems for flow because they dissipate pressure (waste energy) there by making less pressure available for pushing the flow through the downstream capillaries in the heart muscle. In the most clinical situations, the reduction of flow by the stenosis is relevant; however, the angiogram shows only the anatomy of a lesion. The bridge linking anatomy to functional severity is SFR.
- Depending on the physical properties of the blood and by using mathematical equations, it might calculated the most effective physical quantity in the location of the lesion site which is the blood velocity by using the equation (1) on the SFR ratio to find the actual flow we get:

$$(Q_{old} = U_1 A_1) \quad Before\ stenosis \quad \ldots(5)$$

$$(Q_{new} = U_2 A_2) \quad After\ stenosis \quad \ldots(6)$$

$$(Q_{new} = Q_{old}) \quad When:\ 4 \leq SFR \leq 5 \quad \ldots(7)$$

$$\left(Q_{new} = \frac{SFR}{5} Q_{old} \right) \quad When: \ 0 < SFR < 4 \qquad \ldots(8)$$

By using the assumed average flow velocity of (20 cm/s) to be as U_1; and from equations (7) and (8) U_2 will be calculated by the following equations:

$$U_2 = \frac{A_1}{A_2} U_1 \quad When: 4 \leq SFR \leq 5 \qquad \ldots(9)$$

$$U_2 = \frac{4 \times SFR \times A_1}{A_2} \quad When: 0 < SFR < 4 \qquad \ldots(10)$$

3.4. Correlations Between the Obtained Parameters

Based on the obtained data, the following figures are drawn using the Microsoft Office Excel 2007 software.

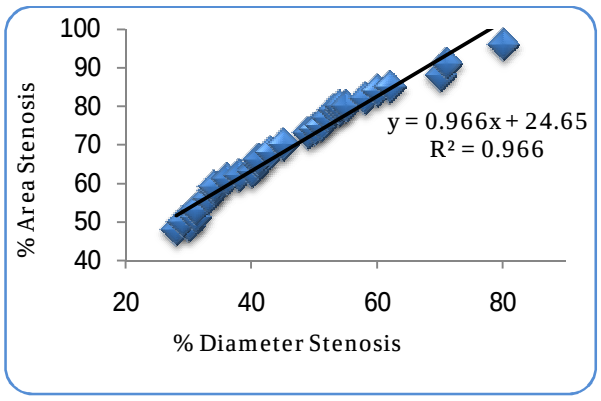

Fig. 2. The Correlation between % Area and % Diameter Stenosis.

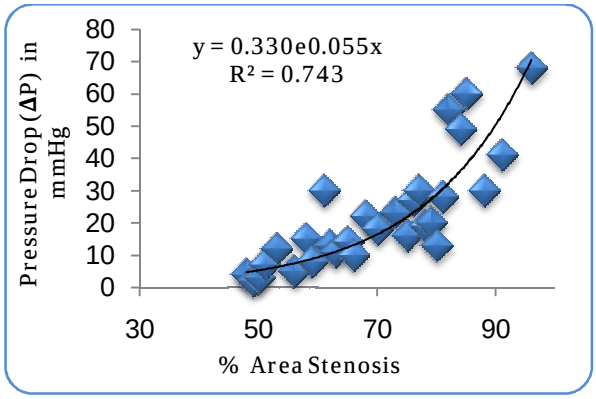

Fig. 3. The Correlation between % Area Stenosis and (ΔP).

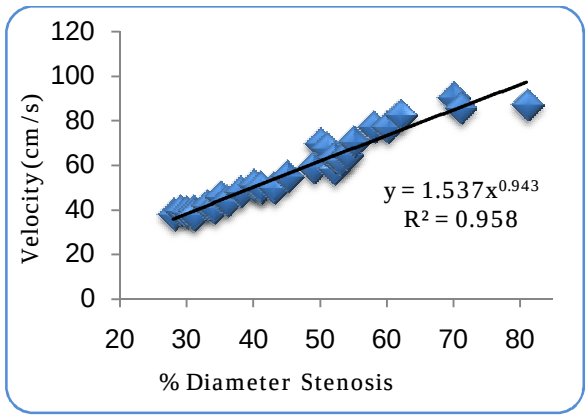

Fig. 4. The Correlation between % Diameter Stenosis and Velocity.

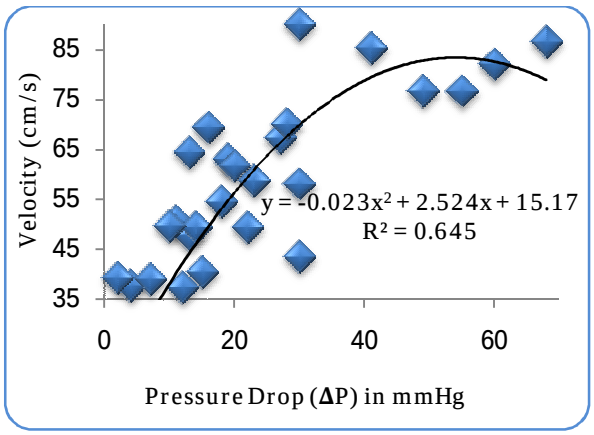

Fig. 5. The Correlation between Velocity and Pressure Drop.

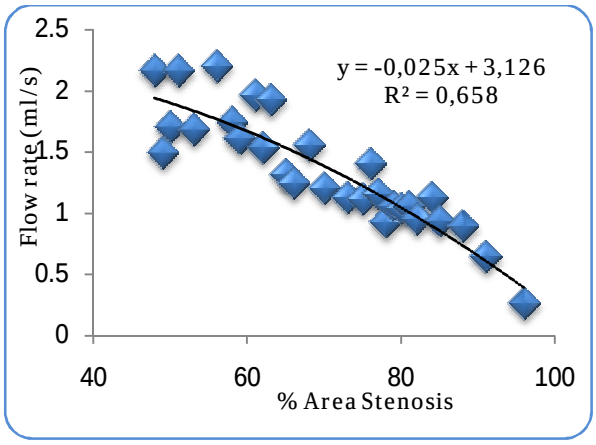

Fig. 6. The Correlation between % area and Blood Flow Rate.

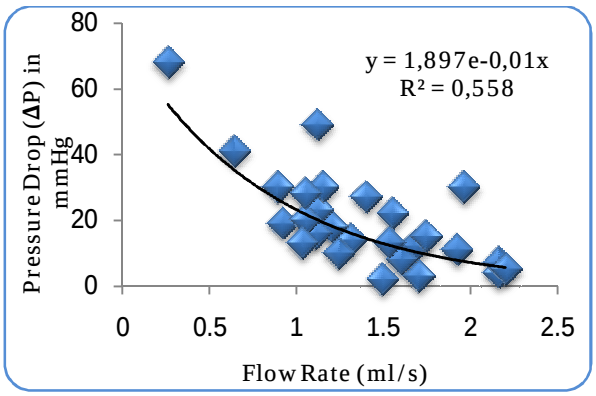

Fig. 7. The Correlation between Blood Flow rate and Pressure Drop (Δp).

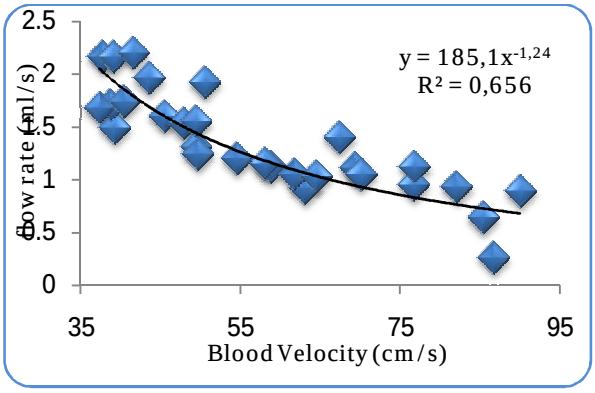

Fig. 8. The Correlation between Blood Flow rate and Velocity at Lesion Site.

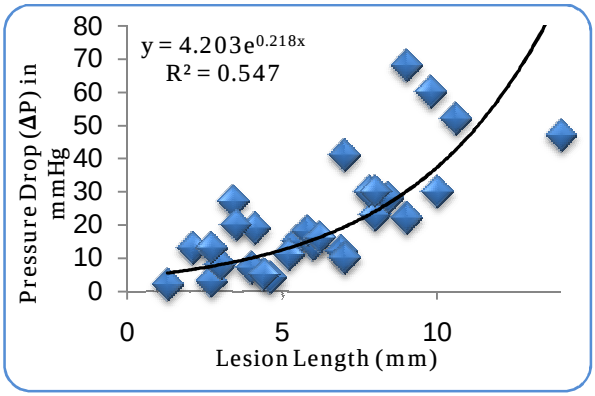

Fig. 9. The Correlation between Lesion Length and Pressure Drop.

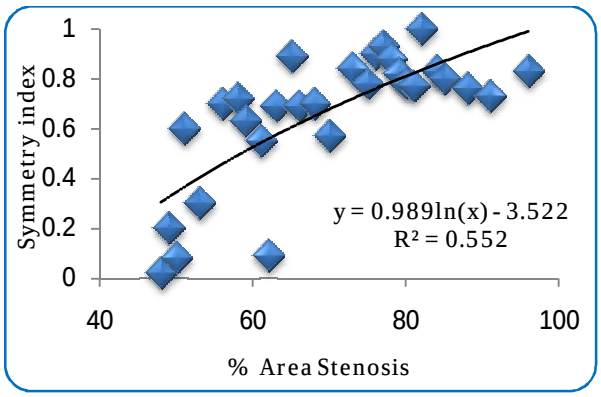

Fig. 10. The Correlation between Symmetry Index and % Area Stenosis.

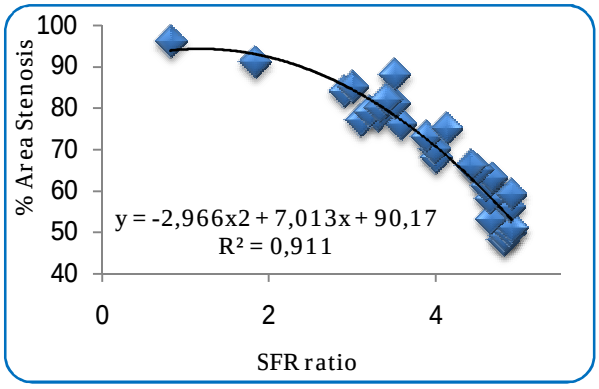

Fig . 11. The Correlation between % area Stenosis and the SFR Ratio.

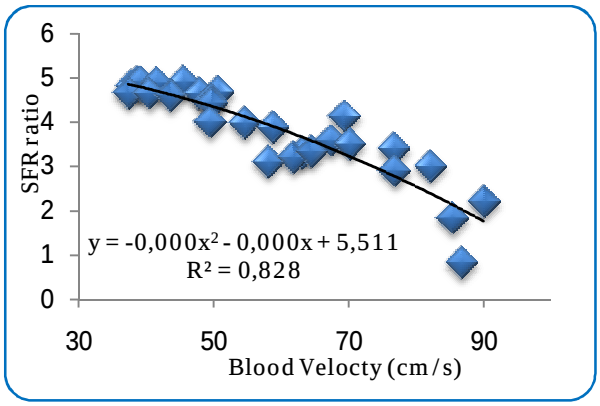

Fig. 12. The Correlation between SFR Ratio and Blood Velocity at Lesion Site.

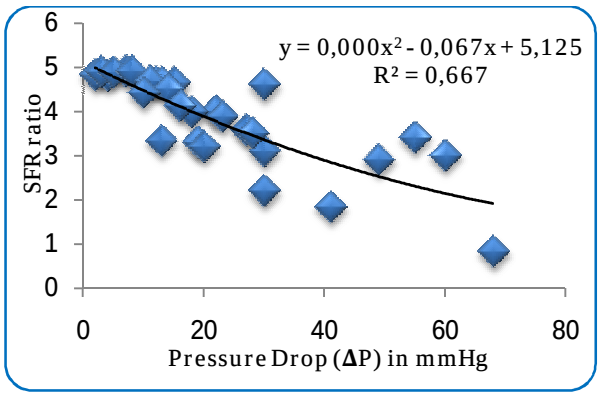

Fig. 13. The Correlation between SFR Ratio and Pressure Drop (Δp).

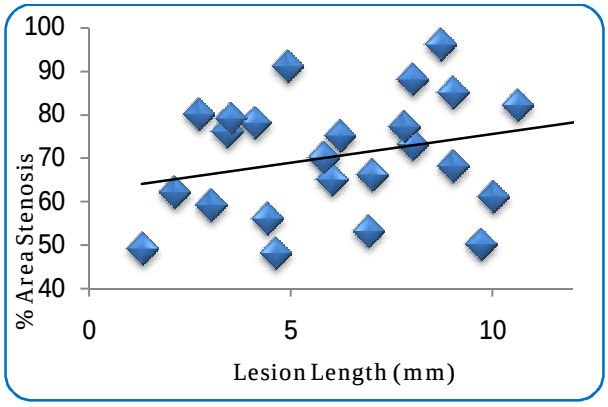

Fig. 14. The correlation between % area stenosis and lesion length.

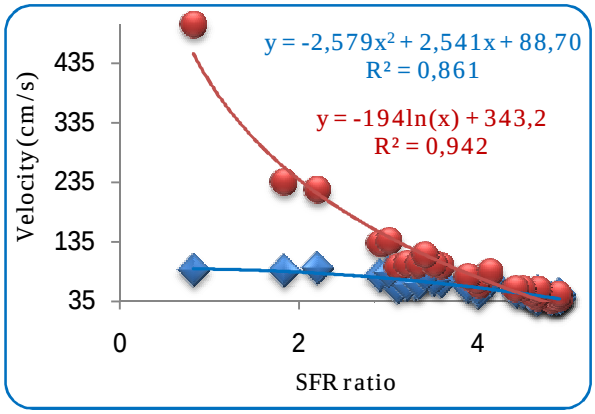

Fig. 15. The Correlation between SFR ratio and Blood Velocity Values by using Equation (7) for all SFR Value, Blue and by using Equation (9 and 10), Red.

4. Theoretical Investigation

4.1. Model Geometry

The geometry under investigation is shown in Figure (16) which is similar to that used in simulation of Griffith et al. [10], in shape and different in dimensions (i.e. the dimensions based on table (2) and (3)) to be more accurate for the simulation of coronary artery. Here; the selected dimensions are in agreement with dimensions of human (LAD) artery, which is the artery under the study, that are taken from the obtained results in previous work.

It consists of a long straight tube with an axisymmetric semicircular constriction. The stenosis degree is defined as: [10]

$$1 - \left(\frac{D_2}{D_1} \right)^2 \times 100\% \qquad \ldots(11)$$

Where D_1 is the internal diameter of the vessel and D_2 is the diameter at the centre of the constriction.

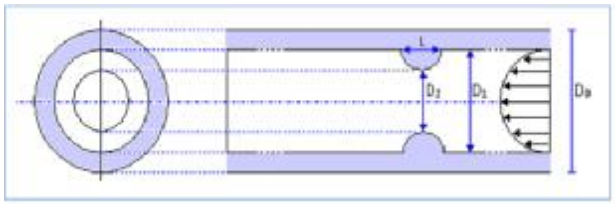

Fig. 16. Schematic Diagram of the Geometry used in this Study.

The internal diameter of the vessel, D_1 is 3mm and the wall has a thickness of 0.5mm, giving an external diameter, D_0 of 4mm.

To achieve proper flow resolution for the simulation, the pre- and post-stenotic regions were chosen to be 3 and 10 diameters (i.e. 9 and 30 mm) long respectively. This will minimize the influence of the upstream and downstream boundary conditions and sufficiently capture the post-stenotic flow features. [9]

Figure (17) shows the mean velocity waveform of coronary blood flow with a 1.0sec period that was used as the inlet velocity conditions in the computational models. It is similar to that used in the simulation of Dehlaghi et al. [3].

The severity of a stenosis or stenosis degree is determined by the amount of the cross sectional area that has been 'blocked' by the occlusion. For stenoses with varying geometry, the cross section is usually taken to be the narrowest portion (referred to as the 'throat') of the blockage.

In this study it will be ≅ 56%; that means D_2 is 2mm in equation (11) and the length of the stenotic portion, L is set to be 1mm that is in agreement with that obtained from angiographical investigation.

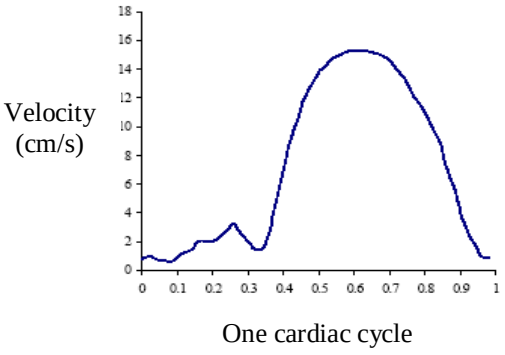

Fig. 17. Physiological Waveform of Pulsatile Coronary Blood Flow that is used as Inlet Velocity of all Models.

4.2. Boundary Conditions

For the fluid model, the vessel walls are assumed to have a no-slip boundary condition applied. Vessel porosity is also ignored; therefore fluid is assumed not to penetrate through the walls as it flows along the vessel. Therefore, the boundary conditions applied to the vessel walls are:

$$u_i = u_j = o \quad \ldots(12)$$

Along the line axis of symmetry, there is to be no change of velocity in the radial direction, effectively reducing the radial component of the velocity to be zero.

Therefore, the boundary condition applied is:

$$u_i = \frac{\partial u_i}{\partial x_i} = o \quad \ldots(13)$$

For validation with literature, a parabolic velocity profile corresponding to a fully developed Poiseuille flow for a Newtonian uncompressible flow through a circular tube was specified. This profile varies with time according to the waveform specified in Figure (20). The maximum velocity Umax(t) of the parabolic profile corresponding to the appropriate flow is equal to two times the mean velocity of the parabolic profile, Umean(t), for laminar flow within a circular tube, i.e.:

$$U_{max}(t) = 2U_{mean}(t) \quad \ldots(14)$$

Due to the changes in viscosity with shear rates, each Newtonian and non- Newtonian model will have different fully developed velocity profiles, which can affect the flow behavior significantly about the stenosis. [10]

For the outlet of the flow model, a constant pressure of 4140 Pa was set for all models. This value was chosen to be as that used by Chan et al. simulation [7].

The solid model corresponding to the vessel walls is assumed to be fixed at the ends such that only movement in the radial-tangential plane is allowed. The outer surface of the vessel is assumed to be at the equilibrium pressure of 0 Pa, which allowed the vessel wall to distend or contract accordingly based on the pressure distributions within. For the inner surface of the vessel, the fluid pressure will be applied to deform the structure.

4.3. Formulation of the Problem

This study will investigate the effects of implementing non-Newtonian models for blood flow as well as having the wall deform following the FSI iterative process. It is important to provide several comparative studies between these factors by comparing fluid properties such as the wall shear stress (WSS), pressure distribution and flow velocity and viscosity distributions. In addition, several simulations need to be run to provide comparison with available literature to determine if the geometry used, the fluid and solid model settings and the FSI method implemented are accurate.

To achieve this validation, there will be one case run: Newtonian pulsatile flow through a rigid wall (Model I). Then; the investigation of pulsatile Newtonian flow through a compliant (FSI-enabled) wall (Model II) is used. And the investigation of pulsatile non-Newtonian flow through the geometry incorporating FSI: Carreau model (Model III) is used to determine the effect of the change in viscosity on the flow behavior.

4.3.1. Rigid Newtonian Model (Model I)

In this simulation the fluid was assumed to be incompressible, meaning the density is set to remain constant, and Newtonian. The vessel wall is set to be non-deformable. Pulsatile flow was specified at the inlet as the waveform which is shown in Figure (17). The velocity profile used for the inlet of this model was a fully developed laminar profile, as mentioned previously. This

allowed the model settings to be similar to that used by Mittal et al. [5]

The fluid was set to have a density of 1050 kg/m^3 and a constant viscosity of 0.00345 N.s/m^2. Also, the maximum and minimum Reynolds numbers (Re) of the model were to be between (760 and 160) respectively. Because of this low Reynolds number and the relatively mild stenosis of the geometry, the flow was assumed to be laminar and reasonably axisymmetrical. For the fluid properties mentioned for this model and the boundary condition, the Womersley parameter ($\propto$) for a 3mm diameter tube has a value of 3.65.

4.3.2. FSI Newtonian Model (Model II)

This model took into consideration the structural response to the flow properties of Model I. Therefore the solid model requires definitions to allow the response to be as realistic as possible. Since this model is also used to provide comparisons to literature results which in turn will validate the FSI iterative scheme and solid-model solver, therefore, the vessel was considered to be incompressible, isotropic and linearly elastic, with a Young's modulus of 500 KPa, a Poisson ratio of 0.499 and a density of 1000 kg/m^3 like the one used by Chan et al. [7]
The geometry used has been extensively discussed in section 4.1, whereas the equations of motion for an elastic solid are given in section 4.2. Ideally, the vessel wall should be modeled as a hyperelastic material, which is the behavior of real tissue. [9]

Due to the fact that small deformations are expected, however, and for solver economy, the solid model was assumed to be isotropic elastic for FSI simulations. The fluid model used was exactly as in the case for Model I. As described in the FSI iterative scheme, the flow will determine the deformation of the solid model, which in turn affects the shape flow path within the vessel.

4.3.3. FSI Carreau Model (Model III)

For this model, the geometry used will be the same as that in Model II, where the solid model conditions are kept the same i.e. isotropic elastic. The fluid model is adjusted that it has same density of 1050 kg/m^3 with new value of viscosity by using Carreau equation to specify the shear rate versus the apparent viscosity, and the rate that the axial velocity rises as one moves from the vessel wall toward the center.

As the Carreau equation is for non-Newtonian fluids that exhibit shear thinning, the equation that describes the viscosity – strain rate $\dot{\gamma}$, is as shown below, with the viscosity μ, given in Poise, P (where 1 P = 0.1 N.s/m2). [8]

$$\mu = \mu_\infty + (\mu_0 - \mu_\infty)[1 + (\lambda\ \dot{\gamma}\ )^2]^{(n-1)/2} \quad \ldots(14)$$

Where, λ = 3.313 s, n = 0.3568, zero strain viscosity (i.e. resting viscosity), μ0 = 0.56 P and infinite strain viscosity, μ∞ = 0.0345 P.

4.4. The Simulation Results

The selected five regions represented in Figure (18-a) illustrate the critical node locations corresponding to IP, BS, MS, AS, and OP, that have node numbers of 247, 232, 216, 6, and 195 respectively. The four different times represented in Figure (18-b) illustrate the different phases of the cardiac cycle: minimum systole flow (t1), acceleration phase (t2), peak diastole (t3), and deceleration phase (t4).

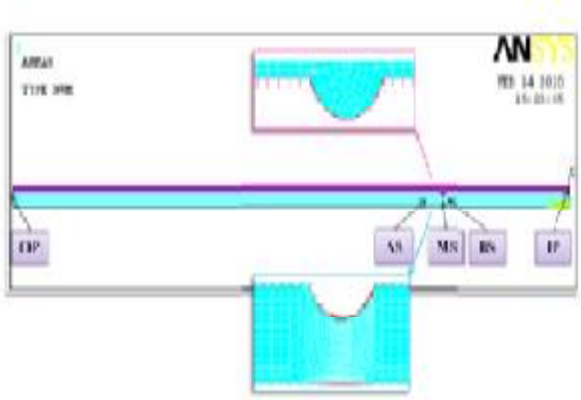

Fig. 18- a. Model Geometry Showing the Fluid (Blue) the Solid (Pink) Models and the Mesh about the Stenotic Region as well as the Critical Node Locations Corresponding to the Inlet and Outlet, Points (IP) and (OP) Respectively, the Pre-Stenotic Region (BS), the Mid-Stenotic Region (MS) and Post-Stenotic Region (AS).

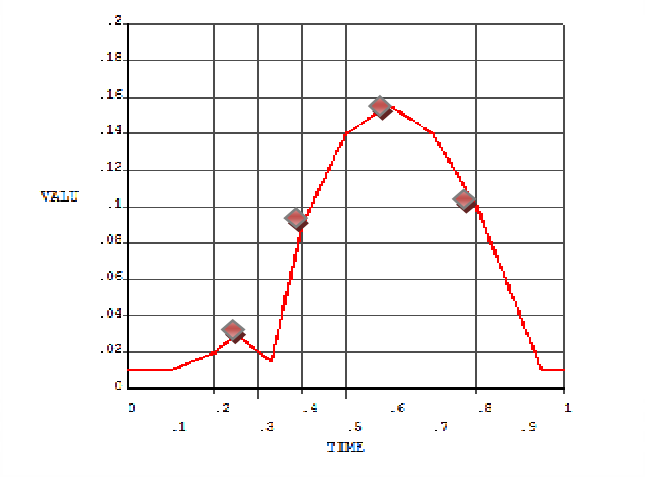

Fig. 18- b. The Input Axial Velocity Waveform for all Coronary Artery Models with four Selected Times; 0.25 s (t_1), 0.40 s (t_2), 0.60 s (t_3), 0.80 s (t_4).

4.4.1. (Model I) Results

- **Centerline Axial velocity**

The centerline axial velocity waveforms for model I in the selected five positions are shown in Figure (19).

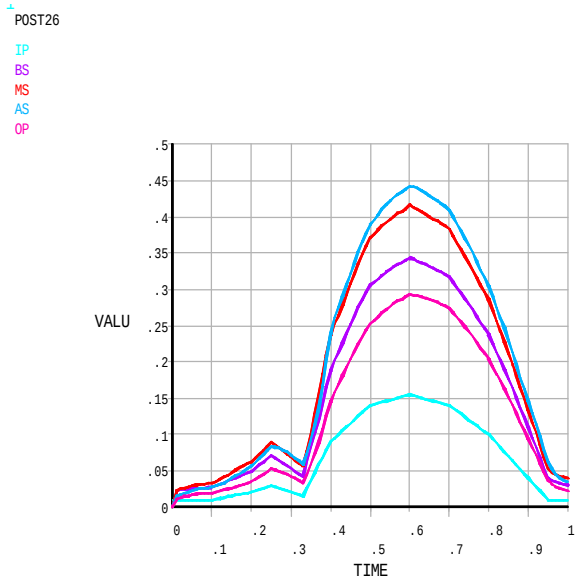

Fig. 19. The Centerline Axial Velocity Waveforms for Coronary Artery Model I with Respect to Time.

The values of the centerline axial velocity in the selected five points at the selected four times are listed in Table (4).

Table 4,
The values of the centerline axial velocity for coronary artery model I in the selected five points at the selected four times.

Point Position	Values of Centerline Axial Velocity (cm/s)			
	t_1	t_2	t_3	t_4
IP	3.000	9.000	15.500	10.000
BS	4. 753	18.293	33.391	23.136
MS	8.368	23.594	41.590	28.590
AS	8.270	23.906	44.261	30.545
OP	4.867	14.967	29.106	20.720

- **Axial Velocity Profile**

The axial velocity profiles were obtained in three sites; BS, MS, and AS at the selected four times and are shown in Figure (20).

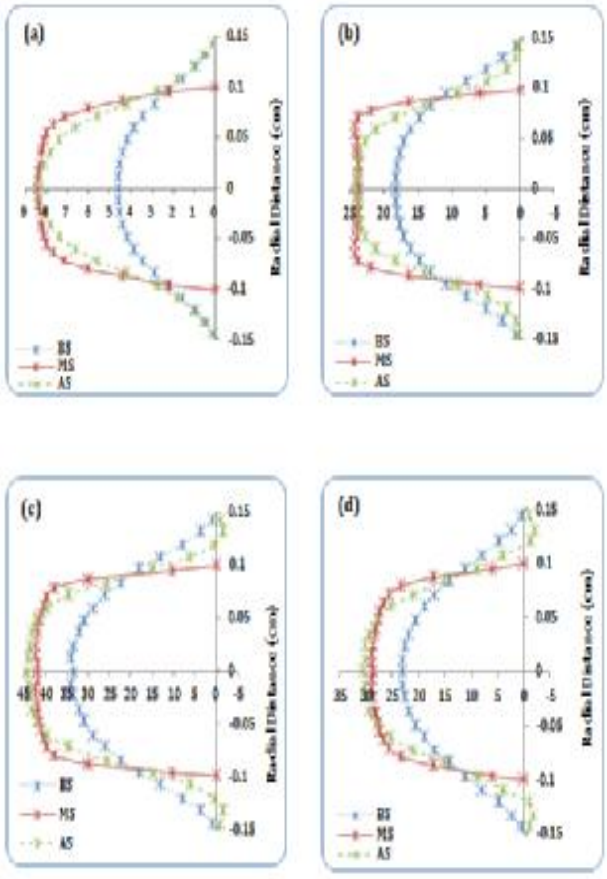

Fig. 20. The Axial Velocity Profiles for Model I in BS, MS, and AS at t1 (a), t2 (b), t3 (c), and t4 (d).

- **The Recirculation Flow Regions**

For model I;the recirculation region and its variation with time are shown in Figure (21).

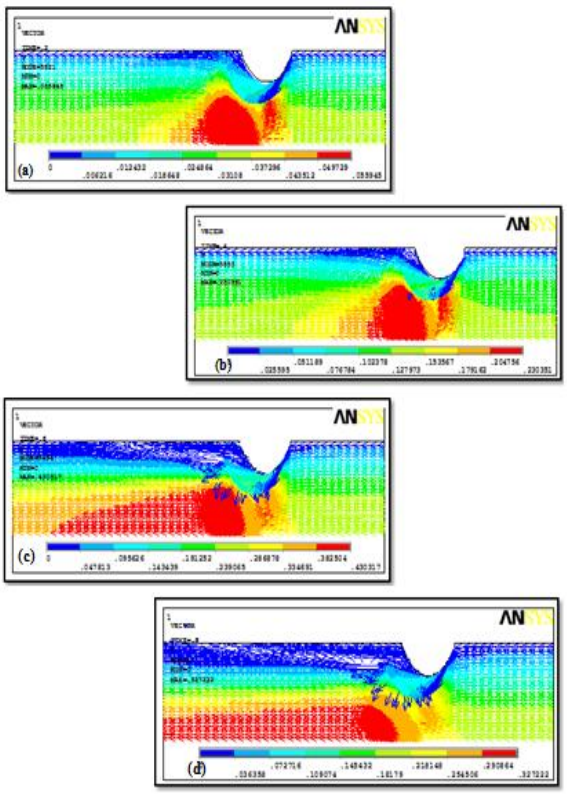

Fig. 21. The Recirculation flow Regions of Model I in t_1 (a), t_2 (b), t_3 (c), and t_4 (d).

- **Pressure Gradient**

The pressure gradient in the selected four times with respect to axial distant for model I is shown in Figure (22).

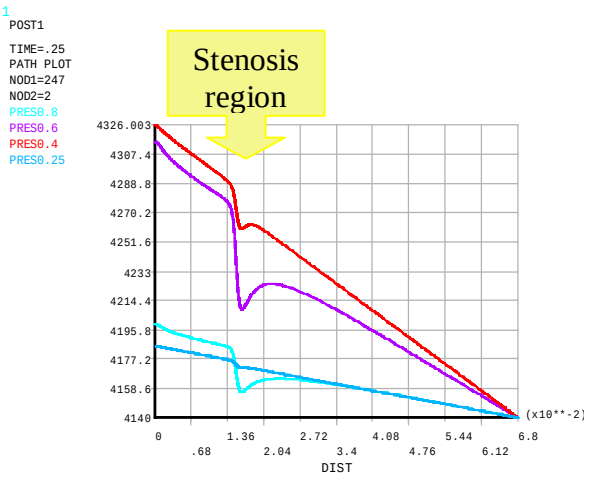

Fig. 22. The Pressure Gradient of Model I at t_1 (blue), t_2 (red), t_3 (violet), and t_4 (green).

At time t_3; i.e. at 0.60 sec, the maximum value of the pressure drop is appeared. The pressure values in the five selected points at t_3 are listed in Table (5).

Table 5,
The values of pressure for model I in the five selected points at t_3.

Point Position	Values of pressure (Pa)
IP	4316.9
BS	4277.7
MS	4212.6
AS	4224.2
OP	4140.0

4.4.2. (Model II) Results

- **Centerline Axial Velocity**

The centerline axial velocity waveforms in the selected five positions for model II are shown in Figure (23).

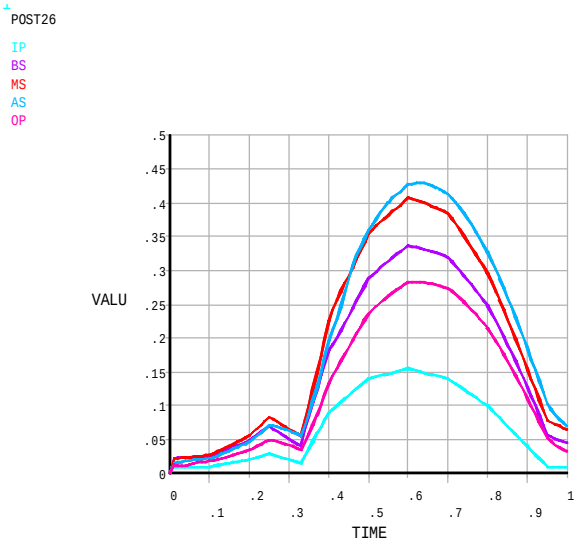

Fig. 23. The Centerline Axial Velocity Waveforms for Coronary Artery Model II with Respect to Time.

The values of the centerline axial velocity in the selected five points at the selected four times are listed in Table (6).

Table 6,
The values of the centerline axial velocity for coronary artery model II in the selected five points at the selected four times.

Point Position	Values of Centerline Axial Velocity (cm/s)			
	t_1	t_2	t_3	t_4
IP	3.000	9.000	15.500	10.000
BS	6.852	17.348	32.718	24.220
MS	8. 769	22.590	40.690	29.648
AS	6.874	19.623	42.671	32.704
OP	4.932	13.785	27.846	21.621

- **Axial Velocity Profile**

The axial velocity profiles were obtained in three sites; BS, MS, and AS at the selected four times and are shown in Figure (24).

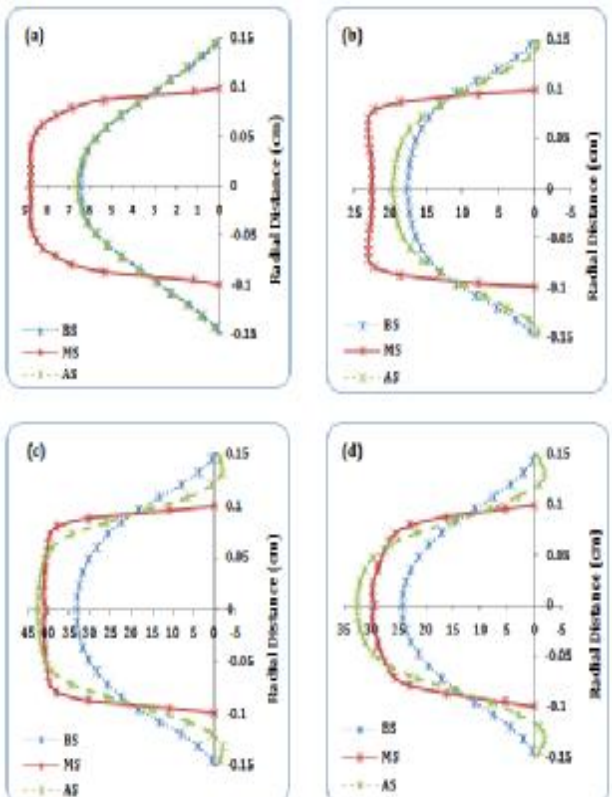

Fig. 24. The Axial Velocity Profiles for Model II in BS, MS, and AS at t1 (a), t2 (b), t3 (c), and t4 (d).

- **The Recirculation Flow Regions**

For model II; the recirculation flow region and its variation with time is shown in Figure (25)

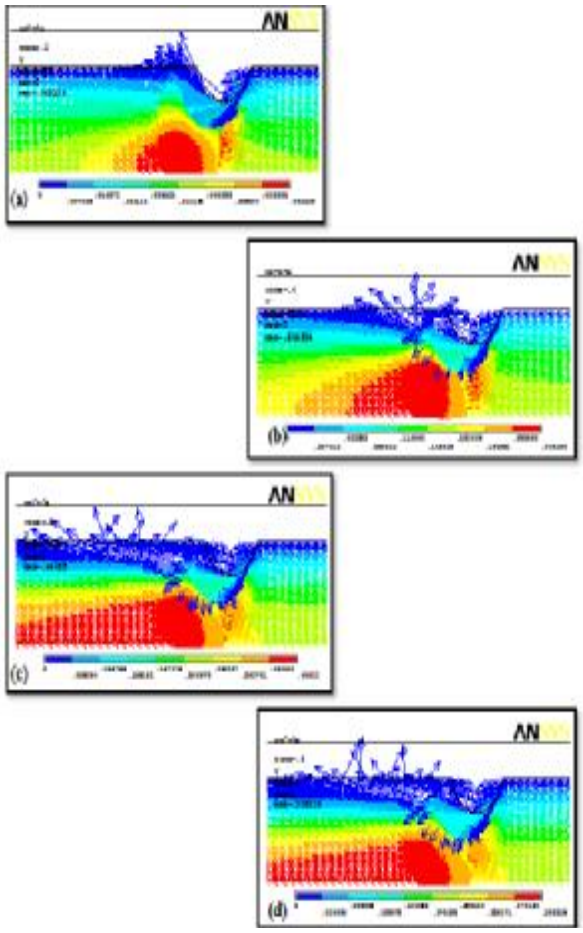

Fig. 25. The Vector Plot of Recirculation Flow Regions for Model II at; t_1 (a), t_2 (b), t_3 (c), and t_4 (d).

- **Pressure Gradient**

The pressure gradient with respect to axial distant in the selected four times for model II is shown in Figure (26).

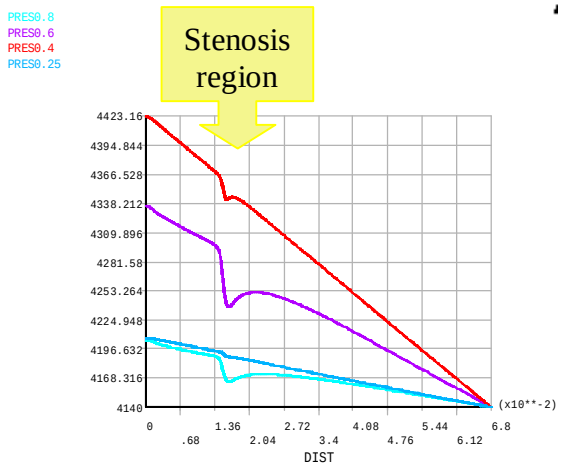

Fig. 26. The Pressure Gradient for Model II at t_1 (blue), t_2 (red), t_3 (violet), and t_4 (green).

At time t_3; i.e. at 0.60 sec, the maximum value of the pressure drop is appeared. The pressure values in the five selected points at t_3 are listed in Table (6).

Table 6,
The pressure values for model II in the five selected points at t_3.

Point Position	Values of pressure (Pa)
IP	4336.8
BS	4295.5
MS	4238.9
AS	4252.8
OP	4140.0

- **Wall Shear Stress (WSS)**

The wall shear stresses in the stenosis site at the selected four times are shown in Figure (27).

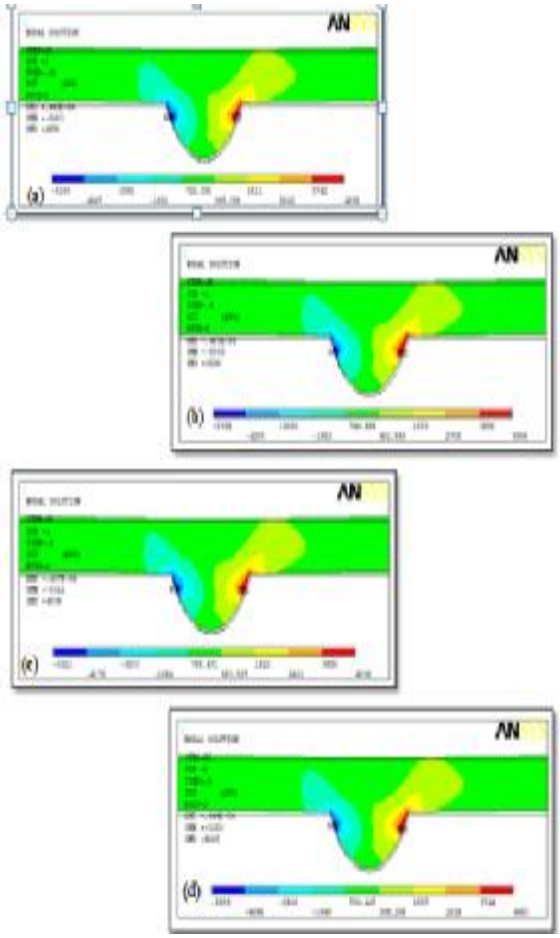

Fig. 27. The Contours of Wall Shear Stress Distribution for Model II at; t_1 (a), t_2 (b), t_3 (c), and t_4 (d).

- **Wall Stress Distributions**

The wall stresses (radial, axial, and circumferential) in the stenosis site at the selected four times are shown in Figure (28).

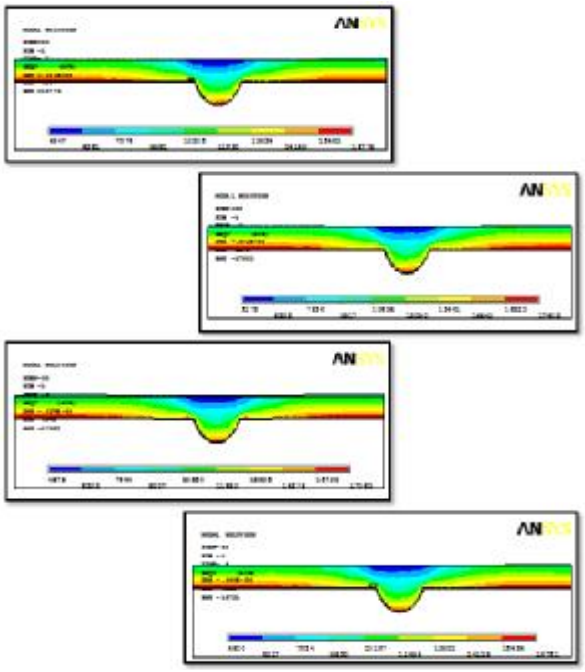

Fig. 28. The Contours of Wall Stress Distribution (Radial, Axial, and Circumferential) for Model II at; t_1 (a), t_2 (b), t_3 (c), and t_4 (d).

4.4.3. (Model III) Results

- **Flow Viscosity Distribution**

The flow viscosity distributions at four instances within one phase of the fluid flow are plotted in Figure (29).

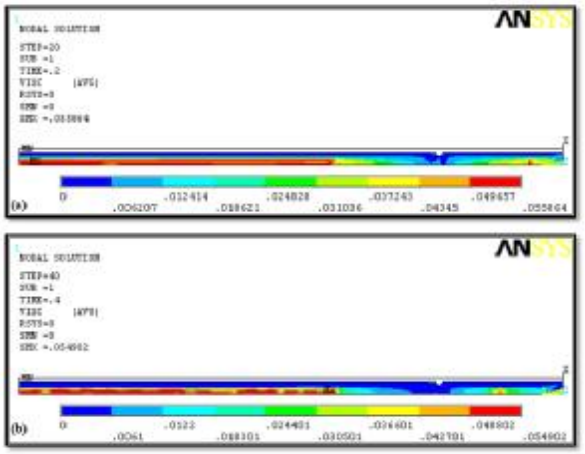

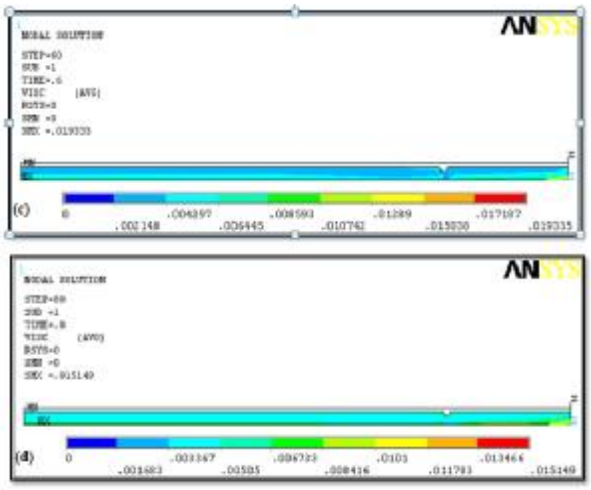

Fig. 29. The Flow Viscosity Distributions for Model III at t1 (a), t2 (b), t3 (c), and t4 (d).

- **Centerline Axial Velocity**

The centerline axial velocity waveforms in the selected five positions for model III are shown in Figure (30).

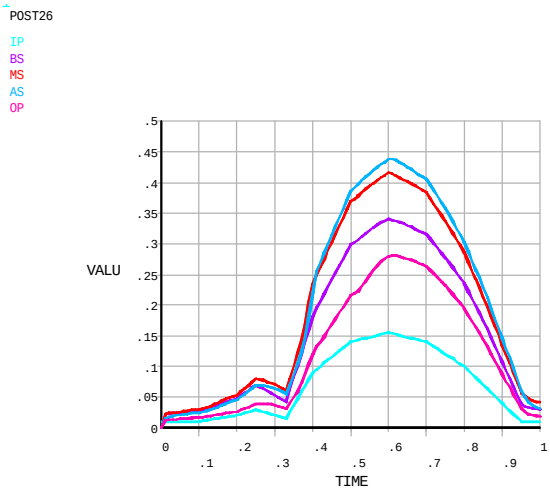

Fig. 30. The Waveforms of the Centerline Axial Velocity in Coronary Artery Model III with Respect to Time.

The values of the centerline axial velocity in the selected five points at the selected four times are listed in Table (5).

Table 5,
The values of the centerline axial velocity for coronary artery model III in the selected five points at the selected four times.

Point Position	Values of Centerline Axial Velocity (cm/s)			
	t_1	t_2	t_3	t_4
IP	3.000	9.000	15.500	10.000
BS	6.773	17.487	33.110	22.875
MS	8.605	23.314	41.802	28.536
AS	6.714	22.258	43.812	30.299
OP	3.876	12.578	27.821	19.469

- **Axial Velocity Profile**

The axial velocity profiles were obtained in three sites; BS, MS, and AS at the selected four times and are shown in Figure (31).

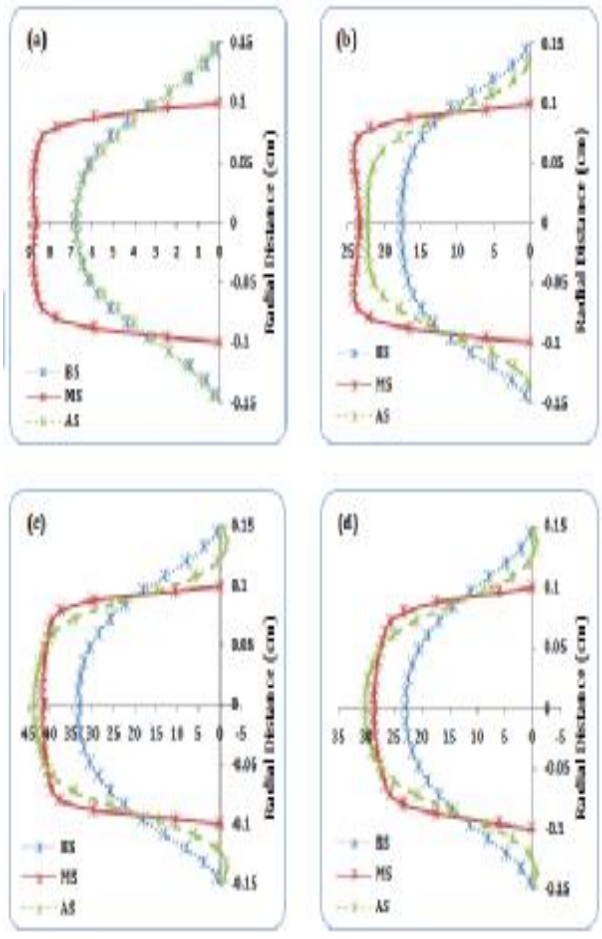

Fig. 31. The Axial Velocity Profiles in BS, MS, and AS for Model III at t_1 (a), t_2 (b), t_3 (c), and t_4 (d).

- **The Recirculation Flow Regions**

For model III; the flow recirculation regions and its variation with time are shown in figure (32).

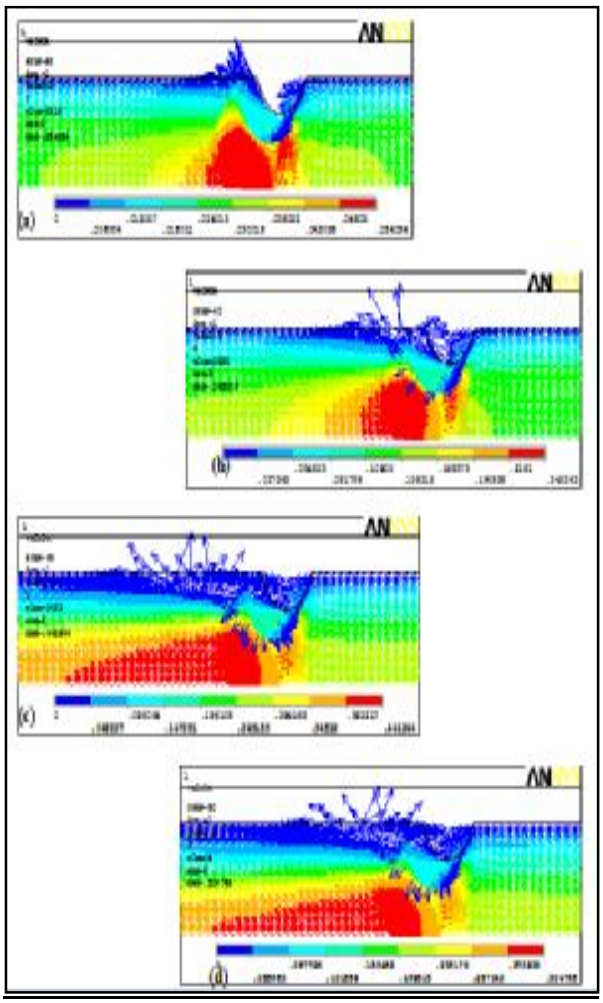

Fig. 32. The Recirculation Flow Regions of Model III in t_1 (a), t_2 (b), t_3 (c), and t_4 (d).

- **Pressure Gradient**

The pressure gradient with respect to axial distance in the selected four times for model III is shown in Figure (33).

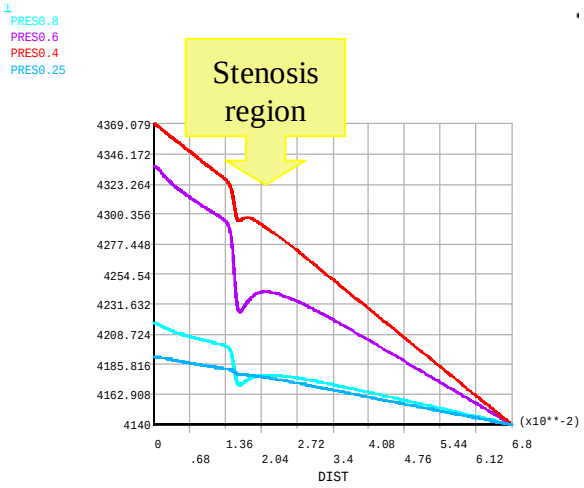

Fig. 33. The Pressure Gradient for Model III at t_1 (Blue), t_2 (Red), t_3 (Violet), and t_4 (Green).

At time t_3; i.e. at 0.60 sec, the maximum value of the pressure drop is appeared. The pressure values in the five selected points at t_3 are listed in Table (6).

Table 6,
The pressure values for model III in the selected five points at t_3.

Point Position	Values of pressure (Pa)
IP	4335.3
BS	4297.4
MS	4229.6
AS	4241.4
OP	4140.0

- **Wall Shear Stress (WSS)**

The wall shear stresses in the stenosis site for model III at the selected four times are shown in Figure (34).

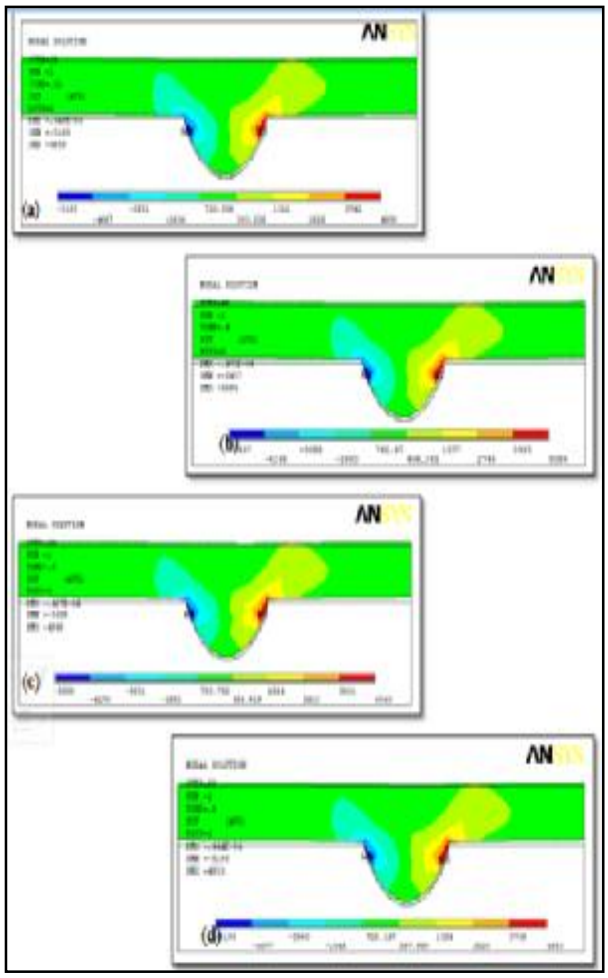

Fig. 34. The Contours of Wall Shear Stress Distribution for Model III at t_1 (a), t_2 (b), t_3 (c), and t_4 (d).

- **Wall Stress Distributions**

The wall stresses (radial, axial, and circumferential) in the stenosis site at the selected four times are shown in Figure (35).

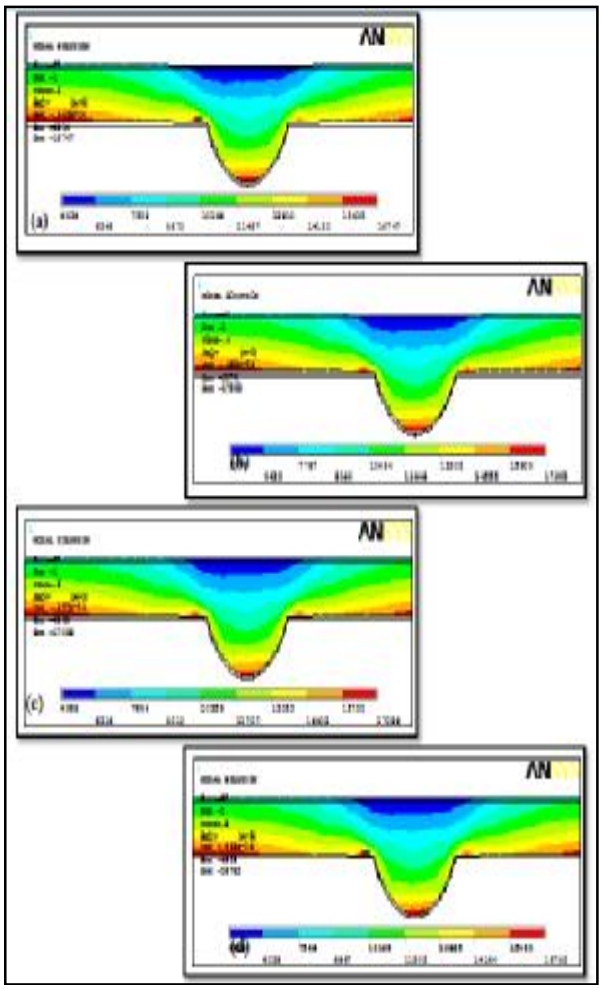

Fig. 35. The Contours of Wall Stress Distribution (Radial, Axial, and Circumferential) for Model III at; t_1 (a), t_2 (b), t_3 (c), and t_4 (d).

5. Conclusions

This study provides some understanding of blood flow characteristics in stenosed artery generally; and in stenosed LAD coronary artery especially when it is affected by atherosclerotic disease.

5.1. Conclusion from the Angiographic Data

The reference diameters of the proximal site of LAD decreases reflecting that the artery is affected with by than 25% diameter reduction was ready to accept the lesions anatomically. The cross-section area as a result for a decrease in diameters is affected more.

A good correlation between % area and diameter stenosis indicates that we can use any of the two quantities to estimate the reduction in the ability of the LAD to achieve its function in supplying blood to most of the anterior part of the heart.

A positive correlation between pressure drop and % area stenosis indicating a relation which leads to the effect of the pressure drop on the % area stenosis.

The relation between the pressure drop and the velocity which is calculated at the lesion site is strong enough to the degree that it affects the flow through the stenosis and cause in a reduction in the amount of blood provided along the rest of the LAD.

The sex of subjects has no significant effect on proximal segment of LAD diameters, the cross-sectional areas and the blood flow rates.

The length of the lesion has no influence on the degree of severity of the atherosclerosis disease.

The estimated value of velocity which is by using equation (10) is more satisfying to be closer to real value.

5.2. Conclusion from the Computational Simulation

There are several discrepancies that arise from the limitations of the program, but these do not affect on the overall conclusions.

The comparisons between rigid (Model I) and FSI (Model II) show a notable difference between the two models, which is that the pressures exerted by the fluid tend to increase the cross-sectional area of the flow, which affectively slows the centerline fluid velocity. The increase in vessel radius also enhances the expansion from the stenosed portion to the non-stenosed region, which increases the flow recirculation occurring post-stenosis. The axial velocity profile for the Carreau model (Model III) shows similar behavior to that of the model II.

The viscosity distributions for the Carreau model show significant non-Newtonian effects occurring about the axis of symmetry, particularly in the pre-stenosis region and in the immediate post-stenosis region, as well as in the wall region immediately post-stenosis where recirculation occurs.

This study has produced high wall stress concentrations about the shoulders of the stenosis and the highest stress occurs in the post-stenosis shoulder that provides an insight into the regions where vessel wall rupture is most likely to occur.

The stenosis itself does not indicate high stresses due to the stiffness of the region. Aside from the

shoulders of the stenosis, the ends of the vessel have the largest deformation, which therefore produces significant stresses.

The pressure distributions for all the models show a constant drop in the pre-stenosis region followed by a sharp drop in the stenosed region which then increases when the flow region expands and is then followed by another pressure drop in the post-stenotic region. During the deceleration phase, though, there is a tendency for an adverse pressure to occur across the vessel. The Carreau model tends to show higher pressure variations from the inlet to the outlet throughout the flow phase than FSI Newtonian model. However, the sharp pressure drop at the stenosed region does not vary between the models and it is a function of the geometry. In the immediate post-stenotic region, however, several different pressure characteristics can be noted between the models, such as the pressure rise in the immediate post-stenotic region.

The wall shear stress distributions for all models are similar. The wall shear stress for the Carreau model tended to have a slightly higher magnitude than the Newtonian model due to the higher viscosity near the vessel wall. In the post-stenosis region the large viscosities in the recirculation regions allow for a higher wall shear stress. Overall, the wall shear stress distributions show similar trends to the Newtonian model, suggesting that the shape is a function of the geometry whereas the magnitudes vary between models. It is noted that FSI has an important role in blood flow in stenotic arteries. Therefore, an accurate description of the magnitude and variation in the WSS is useful for detecting the early stages of vascular lesions

6. Comparison with Literature and Experimental Results

As the first step of analysis of the results, the present numerical computations must be validated with the several experimental and analytical solutions with comparable unsteady laminar flows in constricted tube. The aim of this was to establish the validity of the code and settings used in the study as well as to provide an understanding of the effects of incorporating FSI into the simulation. The numerical results derived from this study were found to be in a significant agreement with that found by Mittal [5] who use the same geometry shape and Chan [7] who use the same assumptions. There is a slight difference with the experimental results obtained by Giddens and Ahmed [13] and [14]; but at all the results remain consistent. This could be due to experimental conditions influencing the results, such as gravity, reading errors and model imperfections as a result of the manufacturing process. The results of this study, however, have are similar to results of Chan [7] and Mittal [5]; therefore a similar conclusion can be made.

The centerline axial velocity and axial velocity profiles of the study show strong agreement with the results of Chan [7] and Mittal [5] for both the rigid and FSI models. This, once more, validates the model and settings used for the study for both cases. About wall shear stress the FSI model shows a trend of under predicting the wall shear stress where as the rigid model tends to over predict the wall shear stress. But in spite of that the magnitudes may differ from literature, the trends are notably similar and indicate that peak wall shear stresses occur at the prethroat of the stenosis and vary with the flow rate.

The stress distributions are similar to the results from literature. However, this study has produced high stress concentrations about the shoulders of the stenosis which is in agreement with the thick-wall theory for internally loaded pressure vessels and the highest stress shown in this study occurs in the post-stenosis shoulder. In the comparison with literature, this is viewed as the most significant stress generated within the model.

The overall conclusion that can be derived from the results is that there is a good agreement between the works of this study and the previous studies, both numerical and experimental, thus validating the geometry and methods used.

7. Referenes

[1] F. Yilmaz and M. Gundogdu (A Critical Review on Blood Flow In Large Arteries; Relevance to Blood Rheology, Viscosity Models, And Physiologic Condition). Korea-Australia Rheology Journal, vol. 20 (4), pp. 197-211. [December 2008].

[2] M. Molla and C. Paul (LES of Physiological Pulsatile Flow in a Model Arterial Stenosis). BSME-ASME International Conference on Thermal Engineering, vol.4, pp. 27-29. Dhaka, Bangladesh. [December 2008].

[3] V. Dehlaghi, S. Najarian and M. Tafazzoli-Shadpour (Effect of Stent Geometry On

Phase Shift Between Pressure and Flow Waveforms in Stented Human Coronary Artery). American Journal of Applied Sciences, vol. 5(4), pp. 340-446. [2008]

[4] Safoora Karimi et al (Simulation of Pulsatile Blood Flow Through Stenotic Artery Considering Different Blood Rheologies). biomedical eng. applications, basis and communication, vol.25,[2013].

[5] R. Mittal, S. Simmons and F. Najjar (Numerical Study Of Pulsatile Flow In A Constricted Channel). Fluid Mechanics Journal, vol. 485, pp. 337-378. Cambridge University Press. [2003]

[6] W. Chan, Y. Ding and J. Tu (Modeling Of Non-Newtonian Blood Flow Through A Stenosed Artery Incorporating Fluid-Structure Interaction). ANZIAM Journal, vol. 47, pp.C507-C523. EMAC. [2007]

[7] B. Johnston, P. Johnston, S. Corney and D. Kilpatrick (Non-Newtonian Blood Flow In Human Right Coronary Arteries: Steady State Simulations). Journal of Biomechanics, vol.37, pp. 709-720. [2004]

[8] Hye, Md. Abdul (Simulation of Transient Blood Flow In Models of Arterial Stenosis and Aneurysm), PhD thesis, University of Glasgow, [2012].

[9] M. Griffith, T. Leweke, M. Thompson and K. Hourigan (Steady Inlet Flow In Stenotic Geometries: Convective And Absolute Instabilities). Fluid Mechanics Journal, vol. 616, PP. 111–133. [2008].

[10] J.D. Bronzino, S.M. Blanchard, and J.D. Enderle (Introduction To Biomedical Engineering). Elsevier Academic. [2005].

[11] D. Kwak (CFD-Mature Technology?). NASA Ames Research Center. NASA Advanced Supercomputing (NAS) Division, Applications Branch. [2006].

[12] D. Giddens and S. Ahmed (Velocity Measurements In Steady Flow Through Axisymmetric Stenoses At Moderate Reynolds Numbers). Biomechanics Journal, vol. 16, pp. 505–516. [1993]

[13] D. Giddens and S. Ahmed (Pulsatile Poststenotic Flow Studies With Laser Doppler Anemometry). Biomechanics Journal, vol.17, pp.695–705. [1994].

دراسة نظرية و عملية لجريان الدم في الشريان القلبي المتضيق

صادق جعفر عباس* فرمان قسيم أحمد زهراء عبد الرحمن محمد*****

**قسم الهندسة الطبية / كلية الهندسة / جامعة النهرين*

***قسم الهندسة / مستشفى دار التمريض*

****قسم هندسة الطب الحياتي / كلية الهندسة الخوارزمي/ جامعة بغداد*

الخلاصة

يعتبر التصلب العصيدي الدهني وأسمه العلمي (Atherosclerosis) من أهم الأمراض التي تصيب الأوعية الدموية وأكثرها شيوعا حيث يسبب تضيق في المساحة الداخلية للوعاء الدموي، لذلك فإن دراسة جريان الدم في الشرايين له من الأهمية اللازمة لجعلنا نفهم العلاقة بين الخصائص الديناميكية لجريان الدم و ظهور هذا المرض في الشرايين الدموية.

في هذه الدراسة ، قد تم استخدام طريقة حسابية تدخل ضمن تقنية واسعة تختص بدراسة ديناميكية الموائع تسمى (Fluid Computational Dynamics) وذلك من اجل دراسة جريان الدم في أحد الشرايين التاجية وهو الشريان الأمامي النازل الأيسر ومختصره العلمي (LAD Coronary Artery) حيث تم اختيار المنطقة الأولى القريبة من منشأ الشريان لتكون قيد الدراسة باعتبارها من أكثر المناطق شيوعاً المعروفة بإصابتها لهذا المرض. لقد تم فحص تأثير نسيج الغشاء الوعائي وطبيعة السائل الدموي على جريان الدم المتذبذب أثناء مروره في شريان تاجي ذي تضيق متماثل مستخدمين برنامج ANSYS 11 من اجل توفير مفهوم أساسي للعوامل البايوميكانيكة المرتبطة بعملية تكون مرض التصلب في الشريان.

ومن أجل إيجاد أبعاد حقيقية و معلومات عن الشريان التاجي قيد الدراسة تفيدنا في رسم موديل اقرب للواقع وأيضا لتحقيق هدف آخر للدراسة و هو البحث عن العوامل الفيزيائية وعلاقاتها المتبادلة التي قد تفسر ظاهرة وجود هذا المرض في الشريان التاجي الأمامي النازل الأيسر في بعض الأشخاص أكثر من غيرهم فقد تم تحليل نتائج معينة يظهرها جهاز القسطرة لحوالي ٥٨ مريضاً كانوا قد أحيلوا لأجراء عملية القسطرة التشخيصية للشرايين التاجية في مستشفيين في بغداد، ٤٣ منهم كانت نتائج الفحص لديهم قد دلت على وجود تضيق في القطر لديهم بنسبة أكثر من ٢٥% وذلك في المنطقة الأولى من الشريان التاجي الأمامي النازل الأيسر، المنطقة قيد الدراسة أما بقية الحالات فكانت نتائجهم دالة على وجود تضييق بنسبة أقل من ٢٥% لذلك تم اعتبارهم مجموعة قياسية لتحقيق المقارنة مع المجموعة الأخرى.

وقد حاولنا استنباط قيم تقريبية لسرعة الدم من خلال هذا التحليل للمعلومات المأخوذة من جهاز القسطرة بعيدة عن تلك التي من اللازم توفرها في حساب السرعة و من خلال عدة معادلات رياضية وقوانين فيزيائية خاصة.